ACSNANO

www.acsnano.org

ARTICLE

Suppressing Subcapsular Sinus Macrophages Enhances Transport of Nanovaccines to Lymph Node Follicles for Robust Humoral Immunity

Yi-Nan Zhang, Wilson Poon, Elana Sefton, and Warren C.W. Chan*

Cite This: https://dx.doi.org/10.1021/acsnano.0c02240

Read Online

ACCESS | Metrics & More | Article Recommendations | Supporting Information

ABSTRACT: **Nanovaccines need to be transported to lymph node follicles to induce humoral immunity and generate neutralizing antibodies. Here, we discovered that subcapsular sinus macrophages play a barrier role to prevent nanovaccines from accessing lymph node follicles. This is illustrated by measuring the humoral immune responses after removing or functionally altering these cells in the nanovaccine transport process. We achieved up to 60 times more antigen-specific antibody production after suppressing subcapsular sinus macrophages. The degree of the enhanced antibody production is dependent on the nanovaccine dose and size, formulation, and administration time. We further found that pharmacological agents that disrupt the macrophage uptake function can be considered as adjuvants in vaccine development. Immunizing mice using nanovaccines formulated with these agents can induce more than 30 times higher antigen-specific antibody production compared to nanovaccines alone. These findings suggest that altering transport barriers to enable more of the nanovaccine to be delivered to the lymph node follicles for neutralizing antibody production is an effective strategy to boost vaccination.**

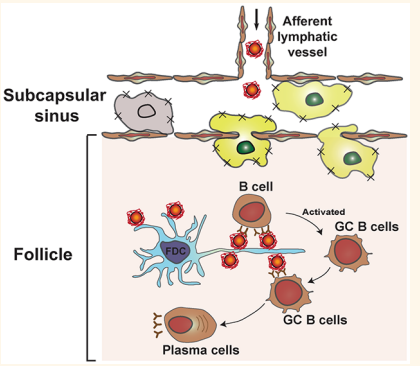

KEYWORDS: *nanovaccine, lymph node, subcapsular sinus macrophages, humoral immunity, antibody, macrophage inhibitor, adjuvant*

Successful vaccinations require antigen delivery into lymph node follicles to generate efficient antibody-mediated humoral immune responses.[1−8] Lymphatic endothelial cells (LECs) form the subcapsular sinus (SCS) floor that only allow smaller antigens (<15 nm) to enter lymph node follicles.[9−11] Macrophages in the SCS area capture larger nanoparticles (>30 nm), immune complexes, viruses, and bacteria and actively transport them to cross the layer of LECs into follicles.[2,12−17] Von Andrian's group reported that CD169$^+$ SCS macrophages translocated surface-bound vesicular stomatitis virus across the SCS floor and presented them to migrating B cells in the underlying lymph node follicles using intravital microscopy.[14] Carrasco and Batista reported that B cells acquired particles and bacteria in a macrophage-rich area at the boundary between the SCS floor and follicle of lymph nodes.[17] Cyster's group also reported that SCS macrophages bind immune complexes on their surface using intravital microscopy.[12] Imaging analysis showed that B cells relayed immune complexes from the subcapsular sinus region to centers of lymph node follicles.[12] These B cells captured immune complexes by a complement receptor-dependent mechanism from SCS macrophages and transported the immune complexes on the surface of follicular dendritic cells (FDCs).[13,18] This principle has been used to target the CD169$^+$ SCS macrophages for effective vaccination.[2,19,20]

Recent studies showed that removing the SCS macrophages did not prevent particle delivery into lymph node follicles and production of humoral immune responses.[21−26] Stevenson's group reported that SCS macrophage depletion with clodronate liposomes increased murine cytomegaloviruses spreading inside lymph nodes and virus production.[25] Von Andrian's group reported that SCS macrophages prevented vesicular stomatitis virus transport to lymph node follicles.[22] Removal of SCS macrophages using clodronate liposomes did not compromise humoral and adaptive immune responses against vesicular stomatitis virus.[22] Iannacone's group con-

Received: March 15, 2020
Accepted: June 1, 2020
Published: June 1, 2020

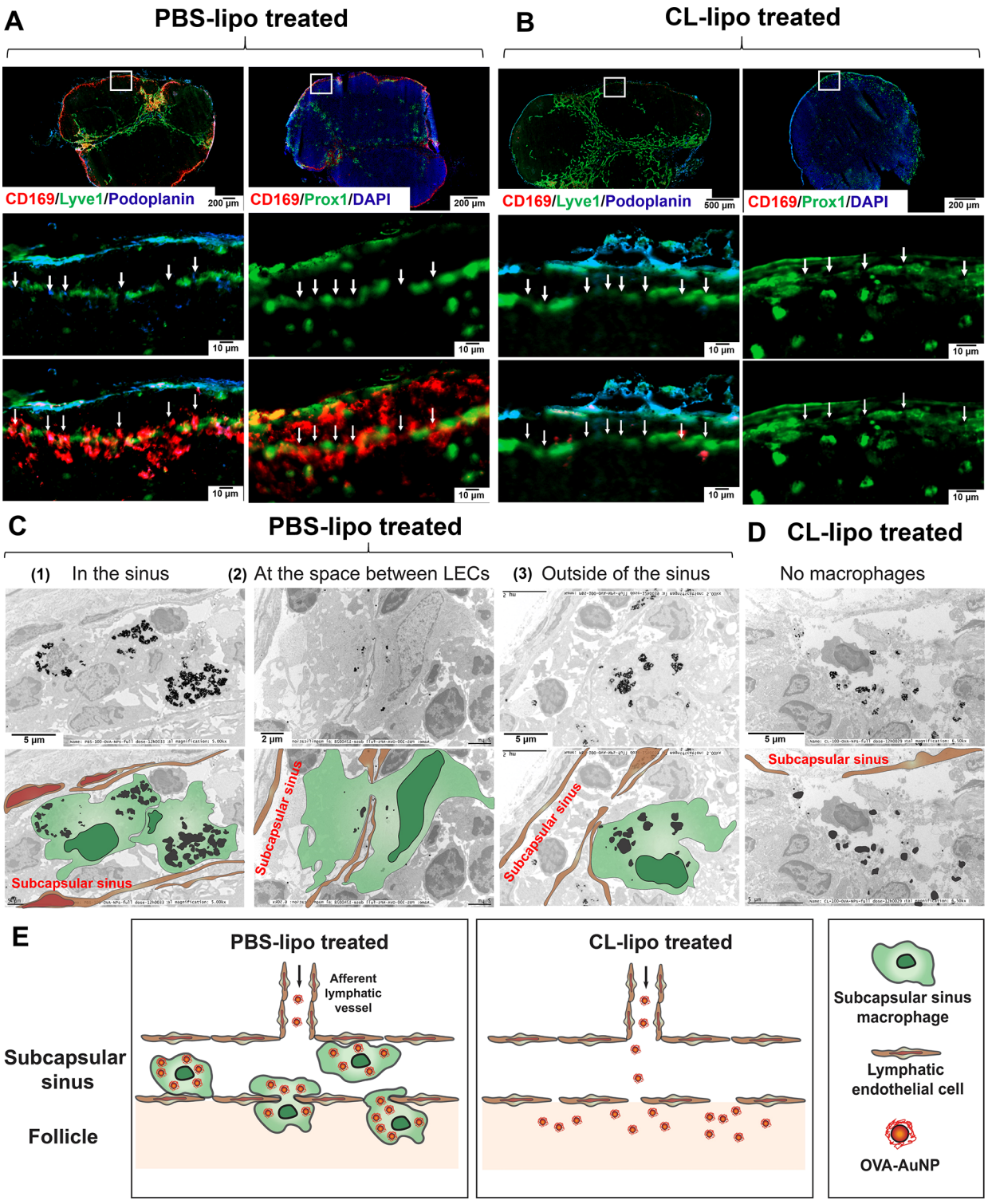

Figure 1. Depleting subcapsular sinus (SCS) macrophages allowed OVA-AuNP nanovaccines to access lymph node follicles. (A) Immunostaining images of the SCS macrophages (CD169, red), lymphatic endothelial cells (Lyve1, green; podoplanin, blue; and Prox1, green). White arrows present the space between LECs. (B) SCS macrophages were depleted with clodronate liposomes in the lymph node, as demonstrated by the lack of CD169 red stain. (C) Representative TEM images of lymph node subcapsular sinus after intradermal footpad injection of 100 nm OVA-AuNP nanovaccines at 12 h. Corresponding schematics were included for better visualization of SCS macrophages (green), LECs (brown), and OVA-AuNP nanovaccines (black). SCS macrophages can sequester nanovaccines when they resided (1) in the lymphatic sinus, (2) at the space between LECs, and (3) outside of the lymphatic sinus and in lymph node follicles. (D) Clodronate liposome treatment depletes SCS macrophages and allows nanovaccines to cross the floor of LECs to access lymph node follicles. (E) Schematic of nanovaccine transport with and without SCS macrophages. PBS-lipo represents PBS liposome, and CL-lipo represents clodronate liposome.

https://dx.doi.org/10.1021/acsnano.0c02240
ACS Nano XXXX, XXX, XXX−XXX

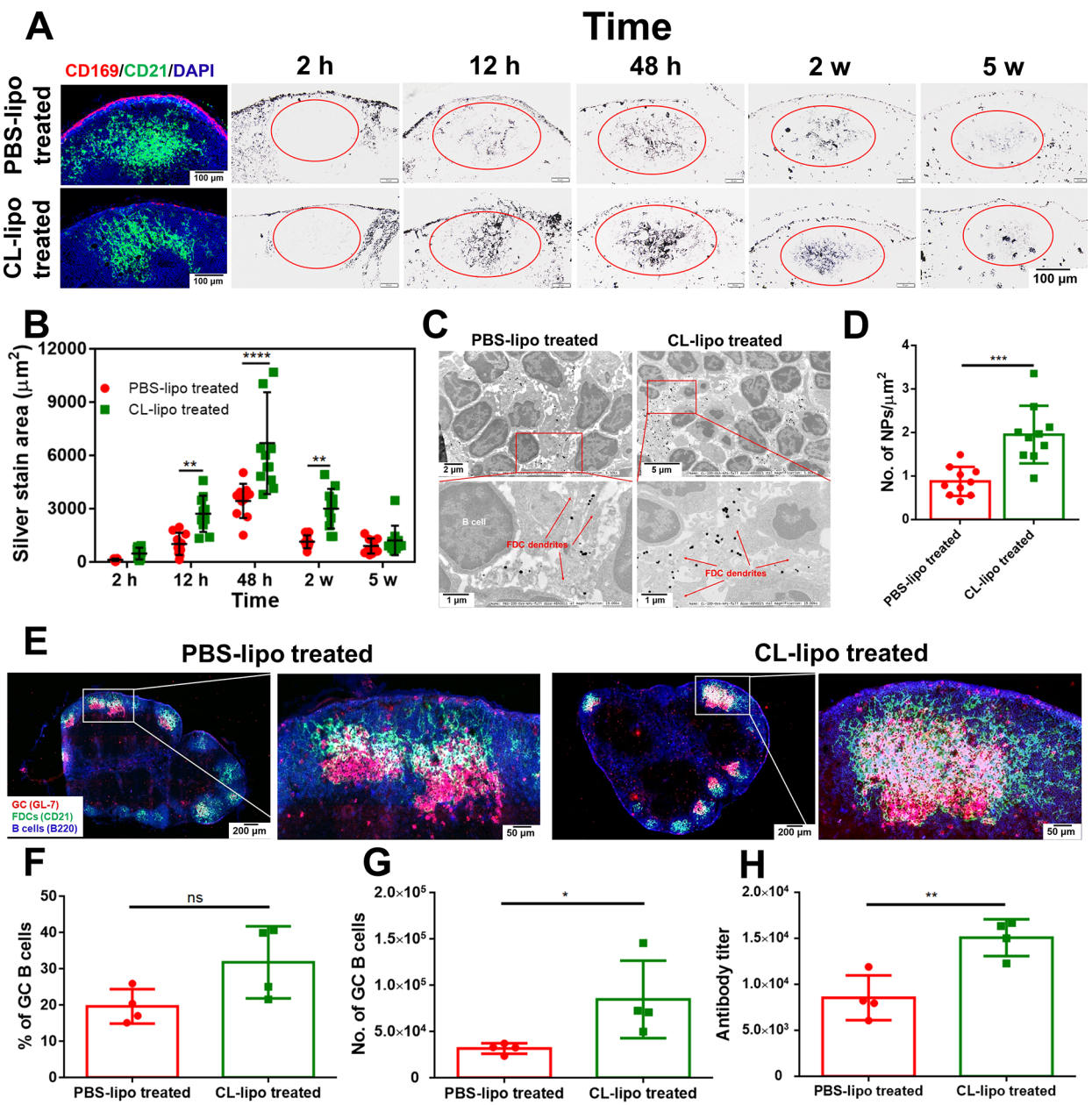

Figure 2. Depleting SCS macrophages increases OVA-AuNP nanovaccine retention and presentation in lymph node follicles and induced greater humoral immune responses. (A) Histological images of lymph node follicles 7 days after intradermal footpad injection of PBS or clodronate liposome treatment. SCS macrophages (red) were depleted after clodronate liposome administration whereas follicular dendritic cells (FDCs, green color) in B cell follicles remained intact. (B) Quantification of 100 nm OVA-AuNP nanovaccine accumulation in follicles at 2 h to 5 weeks 7 days after PBS or clodronate liposome administration. (C) TEM images of 100 nm OVA-AuNP nanovaccine deposition and presentation on the dendrites of follicular dendritic cells (FDCs) at 48 h after intradermal footpad injection 7 days after PBS and clodronate liposome administration. Red arrows point to the dendrites of FDCs. (D) Quantifying numbers of 100 nm OVA-AuNP nanovaccines on FDC dendrites at 48 h. Assessment of humoral immune responses including (E) germinal center formation (GL7 red; CD21 green; B220 blue), (F) percentage of germinal center B cells ($GL7^+B220^+$), (G) numbers of germinal center B cells ($GL7^+B220^+$), and (H) antigen-specific antibody production from blood serum after intradermal footpad injection of PBS and clodronate liposomes 7 days prior to 100 nm OVA-AuNP nanovaccine injection at 5 weeks (n = 4 mice/group). PBS-lipo represents PBS liposome, and CL-lipo represents clodronate liposome. Data shown as mean ± SD; ns: not significant; *P < 0.05; **P < 0.01; ***P < 0.001; ****P < 0.0001. All P values are from two-way ANOVA followed by Tukey's multiple comparisons tests or an unpaired t test.

firmed these findings, reporting that the removal of SCS macrophages using bisphosphonates and clodronate liposomes increased humoral immunity and antibody responses to live and inactive viruses, proteins, haptens, and existing commercial vaccine formulations.[24] Pittet's group reported that SCS macrophages suppress melanoma and prevent tumor-derived extracellular vesicles from entering follicles in the tumor draining lymph nodes.[26] Removal of SCS macrophages using clodronate liposomes promoted tumor-derived extracellular vesicles interacting with B cells and mediated tumor-promoting humoral immunity.[26] More antibody productions were also found in the CD169 knockout mice than wild-type mice.[26] These studies suggested that the removal of SCS macrophages promotes humoral immune responses.

https://dx.doi.org/10.1021/acsnano.0c02240
ACS Nano XXXX, XXX, XXX−XXX

These contradictory findings raise a question: do SCS macrophages promote or prevent nanoparticle or nanovaccine transport to lymph node follicles for humoral immune responses? This question cannot be fully answered from the above-mentioned studies. Imaging analysis using intravital microscopy demonstrated that the SCS macrophages transport the nanoparticles to migrating B cells and FDCs in follicles. However, we do not know if the nanoparticles can be delivered to the FDCs in follicles after depleting or suppressing SCS macrophages. The correlation among SCS macrophages, nanovaccine delivery and retention in follicles, and humoral immune responses is unclear. In this study, we systemically assessed the role of SCS macrophages and their contribution on delivery of nanovaccines to lymph node follicles and to the production of antibodies. The outcomes of this fundamental study will guide the design of vaccine strategies.

RESULTS AND DISCUSSION

Depleting SCS Macrophages Allows More OVA-AuNP Nanovaccines to Access Lymph Node Follicles. Our first set of experiments involved the complete removal of SCS macrophages. Clodronate liposomes have been shown to remove SCS macrophages without depleting other cell populations in lymph nodes (Figure S1).[26−29] We intradermally injected 20 μL of PBS or clodronate liposomes in the footpad of C57BL/6 mice. The amount of injected clodronate drug encapsulated in liposomes is 0.1 mg. We sacrificed the mice 7 days after PBS or clodronate liposome administration and collected the axillary, brachial, and popliteal as sentinel lymph nodes for histological analysis (Figure 1A,B). Lymph node sections were stained using antibodies. Anti-CD169 (red color) was used to stain SCS macrophages. Anti-Lyve1 (green), antipodoplanin (blue), and anti-Prox1 (green) were used to stain LECs. We found that LECs form the lymph node subcapsular sinus with discontinuous cell connections at the sinus floor (Figure 1A,B). White arrows show the space between LECs. The space size is about 1−10 μm (Figure S2). There were no statistically significant differences in space size between PBS liposome and clodronate liposome treatments. SCS macrophages are resident cells located in the sinus or sitting at the interendothelial space of the sinus floor. Some SCS macrophages can be located outside of the sinus and in the B cell follicles. PBS liposome treatment had no influence on macrophage populations, whereas clodronate liposomes depleted SCS macrophages. In both treatments, the sealed interendothelial cell spaces remained open. We conclude that clodronate liposome treatment eliminated SCS macrophages without disrupting the lymph node subcapsular sinus structure.

We next tested if SCS macrophage depletion would affect nanovaccine localization inside or outside of lymph node follicles (Figure 1C,D, and Figure S3). Our nanovaccine model is composed of ovalbumin (OVA) antigen conjugated to spherical gold nanoparticles (AuNPs). OVA is a reference protein and has been widely used as an antigen for vaccination experiments. The full characterization of OVA-AuNP nanovaccine physicochemical properties is described in Figure S4 and Table S1. The rationale of choosing AuNPs is because they are easily synthesized with excellent size control, biocompatible and nonbiodegradable, and easily coated with multiple model antigens.[30] We previously determined that 100 nm OVA-AuNP nanovaccines transport from the injected site to sentinel lymph nodes through the lymphatic system and have the highest follicle retention and OVA-specific antibody production.[30] In this study, we studied 100 nm OVA-AuNP nanovaccine tissue location after PBS or clodronate liposome treatments. We injected 100 nm OVA-AuNP nanovaccines intradermally into the footpad 7 days after intradermal footpad injection of PBS or clodronate liposomes. The injected 100 nm OVA-AuNP nanovaccine dose is normalized based on the injected OVA antigen amount (10 μg) (Figures S4 and S5 and Table S1). The sentinel lymph nodes were collected 12 and 48 h after OVA-AuNP nanovaccine injection (Figure 1C,D, and Figure S6A,B). The morphology of the lymph node subcapsular sinus and OVA-AuNP location in tissue sections were imaged using transmission electron microscopy (TEM). SCS macrophages are the main phagocytic cells that sequestered a major amount of nanovaccines in the subcapsular sinus. They contain prominent electron-dense lysosomes. LECs make up the epithelium of the subcapsular sinus. They have a cobblestone-like appearance. We pseudocolored SCS macrophages in green, LECs in brown, and OVA-AuNP nanovaccines in black for better visualization. TEM images revealed that SCS macrophages can reside (1) in the lymphatic sinus, (2) at the space between LECs, and (3) outside of the lymphatic sinus and in the lymph node follicle (Figure 1C). SCS macrophages are capable of sequestering OVA-AuNP nanovaccines in all locations. Clodronate liposome treatment eliminated SCS macrophages in the above-mentioned positions and allowed OVA-AuNP nanovaccines to cross the floor of LECs to access lymph node follicles (Figure 1D). We illustrated a schematic to demonstrate this phenomenon (Figure 1E). We conclude that SCS macrophages play a barrier role to prevent OVA-AuNP nanovaccines from accessing lymph node follicles.

Depleting SCS Macrophages Increases OVA-AuNP Nanovaccine Retention and Presentation in Lymph Node Follicles and Induces Greater Humoral Immune Responses. We studied the effect of SCS macrophage depletion on OVA-AuNP nanovaccine follicle delivery and humoral immune responses. We determined the kinetics of 100 nm OVA-AuNP nanovaccine accumulation in lymph node follicles after various injection times (2 h to 5 weeks). PBS or clodronate liposomes were injected intradermally into the footpad of mice 7 days before OVA-AuNP nanovaccine administration. Histological images of lymph node follicles revealed that $CD21^+$ FDCs (green color) remained intact in the B cell follicles after clodronate liposome administration indicating that the treatment is specific for the depletion of $CD169^+$ SCS macrophages (red color) (Figure 2A). The gold nanoparticle signal was enhanced by silver staining. We observed a clear difference between clodronate liposome and PBS liposome pretreatments on OVA-AuNP accumulation in lymph node follicles (Figure 2A). Clodronate liposome pretreatment led to faster follicle delivery at 12 h, greater follicle accumulation at 48 h to 2 weeks, and longer retention time of OVA-AuNPs in follicles compared to PBS liposome pretreatment (Figure 2B). From our previous study, we knew that FDCs in lymph node follicles determine OVA-AuNP nanovaccine retention and antigen presentation for B cell activation.[30] TEM images revealed that there was an increase of 100 nm OVA-AuNP deposition and presentation on the FDC dendrites at 48 h in clodronate liposome pretreatment as compared to the control condition (Figure 2C,D and Figure S6C,D). This indicated that more 100 nm OVA-AuNP nanovaccines can stimulate B cell activation after clodronate liposome treatment. We next tested if clodronate liposome

https://dx.doi.org/10.1021/acsnano.0c02240
ACS Nano XXXX, XXX, XXX−XXX

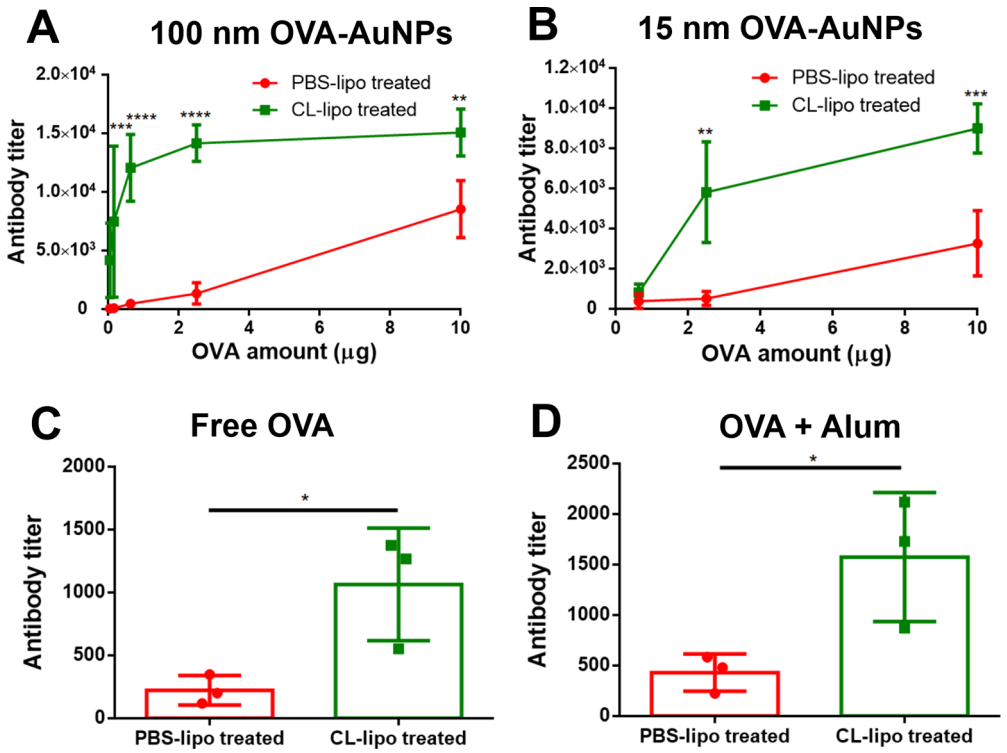

Figure 3. Depleting SCS macrophage allowed greater antigen-specific antibody production in various vaccine designs. Measurements of OVA-specific antibody production after administration of (A) 100 nm and (B) 15 nm OVA-AuNP nanovaccine with (PBS-lipo treated) and without (CL-lipo treated) SCS macrophages. The antigen-specific antibody production was also examined for (C) free antigen and (D) antigen formulated with the commercial adjuvant Alum with wild-type and depleted SCS macrophages (n = 3−6 mice/group). PBS-lipo represents PBS liposome and CL-lipo represents clodronate liposome. Data shown as mean ± SD; *P < 0.05; **P < 0.01; ***P < 0.001; ****P < 0.0001. All P values are from two-way ANOVA followed by Tukey's multiple comparisons tests or an unpaired t test.

pretreatment could induce greater humoral immune responses compared to PBS liposome pretreatment. We immunized the mice using 100 nm OVA-AuNP nanovaccines after PBS or clodronate liposome treatment and sacrificed the mice at 5 weeks. We performed histological analysis for germinal centers using an anti-GL7 stain. Our results showed that 100 nm OVA-AuNP nanovaccines could induce germinal centers (red color) that were attached to the FDC networks (green color) for both PBS and clodronate liposome pretreatments (Figure 2E). We further quantified the percentage and total number of germinal center B cells ($GL7^+B220^+$) after disaggregation of sentinel lymph nodes into single cells for flow cytometry (Figure 2F,G and Figure S7). We found that the clodronate liposome pretreatment generated 2 times more germinal center B cells than PBS liposomes pretreatment. Next, we quantified the amount of OVA-specific antibody production from the blood serum using enzyme-linked immunosorbent assay (ELISA) to determine if clodronate liposome pretreatment elicited greater antigen-specific antibody production. We determined that clodronate liposome pretreatment can induce 2 times more OVA-specific antibody than PBS liposome pretreatment (Figure 2H). We conclude that SCS macrophages are a barrier that prevents OVA-AuNP nanovaccine retention and presentation in lymph node follicles that limits humoral immune responses.

Depleting SCS Macrophages Allows Greater Antigen-Specific Antibody Production in Various Vaccine Designs. We tested if this principle of eliminating the SCS macrophage is applicable to various vaccine designs. We studied the effect of OVA-AuNP nanovaccine dose and size and vaccine formulation on antigen-specific antibody production after elimination of SCS macrophages. We immunized the mice using different doses of 100 nm OVA-AuNP nanovaccine after PBS or clodronate liposome pretreatment and measured the OVA-specific antibody production from blood serum at 5 weeks (Figure 3A). We found that decreasing the 100 nm OVA-AuNP injection dose (normalized based on antigen OVA amount from 10 to 0.04 μg) led to decreased OVA-specific antibody production after PBS liposome pretreatment. Surprisingly, lowering the 100 nm OVA-AuNP nanovaccine injection dose led to nonlinearly decreased antibody production after clodronate liposome pretreatment. Antigen-specific antibody production was improved by 2−60 times after clodronate liposome pretreatment compared to PBS liposome pretreated condition at various 100 nm OVA-AuNP nanovaccine injection doses. After clodronate liposome pretreatment, we could achieve the same OVA-specific antibody production by reducing the injected dose of 100 nm OVA-AuNP by 16 times compared to the injected dose of 10 μg of normalized OVA. SCS macrophage preferred to take up larger particles (>30 nm), such as viruses, bacteria, and immune complexes. We asked if this principle of depleting macrophages can be applied for other nanovaccine designs of a smaller size. We then tested another size of 15 nm OVA-AuNP nanovaccines and found that they followed a similar dose-dependent behavior (Figure 3B). OVA-specific antibody production was significantly higher in response to clodronate liposome than PBS liposome pretreatment. SCS macrophages take up all types of particles, including the soluble antigens, immune complexes, viruses, and bacteria.[2,31] We further tested

https://dx.doi.org/10.1021/acsnano.0c02240
ACS Nano XXXX, XXX, XXX−XXX

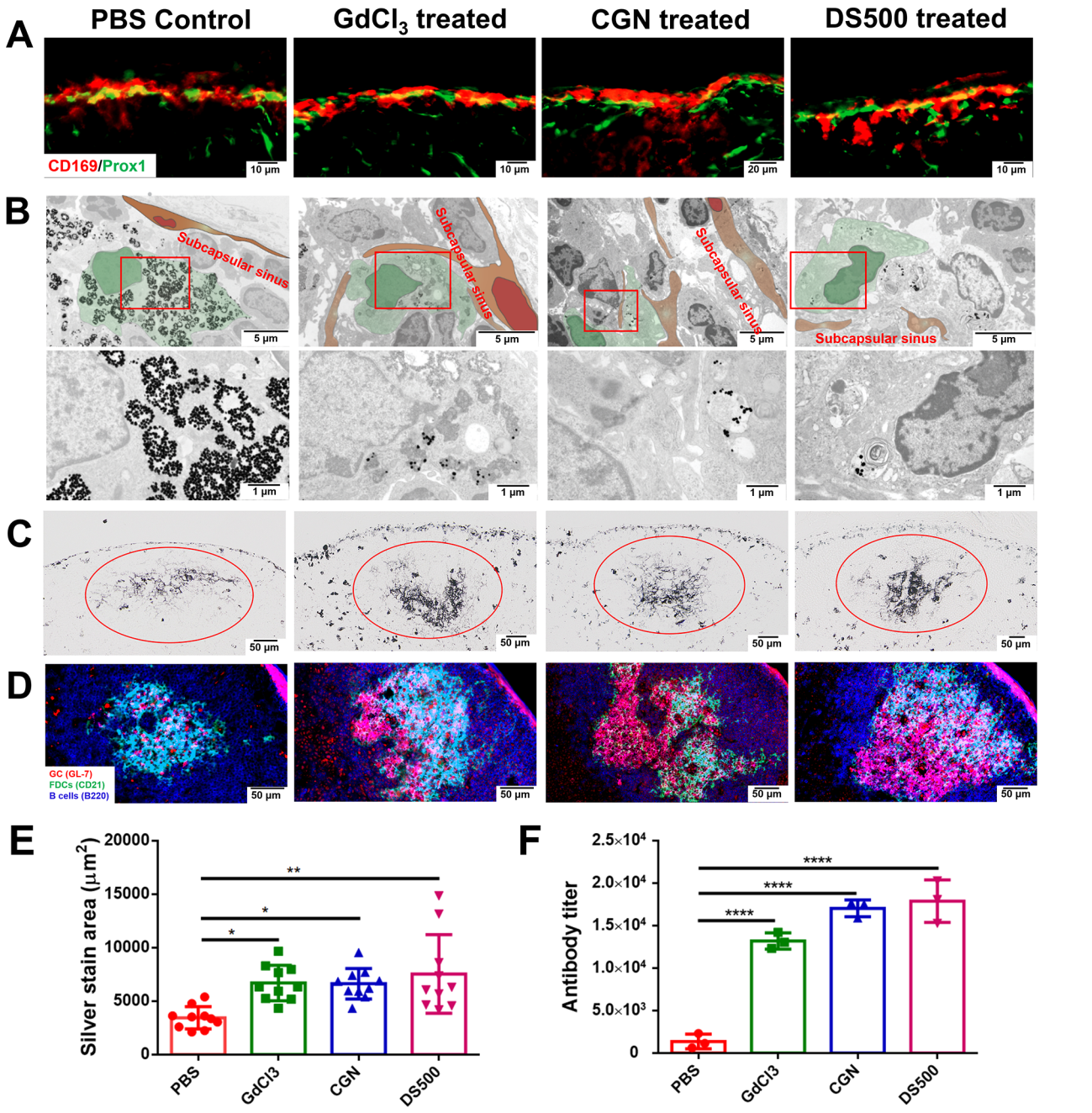

Figure 4. Inhibition of macrophage uptake function improved nanovaccine delivery to lymph node follicles and robust humoral immune responses. (A) SCS macrophages remain intact in the subcapsular sinus of lymph nodes after administration of macrophage inhibitors using $GdCl_3$, carrageenan (CGN), or Dextran sulfate 500. CD169 (red color) stains for SCS macrophages, and Prox1 (green color) stains for LECs. (B) Representative TEM images and the enlarged images of SCS macrophages were examined after intradermal footpad injection of 100 nm OVA-AuNP nanovaccines 24 h after macrophage inhibition administration. SCS macrophages labeled green, and LECs labeled brown. Pretreatment of macrophage inhibitors induces greater 100 nm OVA-AuNP nanovaccine accumulation in lymph node follicles and humoral immune responses (C–F). (C) Histological images of 100 nm OVA-AuNP nanovaccine accumulation in lymph node follicles were analyzed 48 h after nanovaccine intradermal footpad injection. Macrophage inhibitors were administered 24 h prior to nanovaccine injection (n = 4 mice/group). (E) Quantification of 100 nm OVA-AuNP nanovaccine accumulation in follicles at 48 h after macrophage inhibitor administration. Assessment of (D) germinal center formation (GL7 red; CD21 green; B220 blue) and (F) antigen-specific antibody production in blood serum after administration of 100 nm OVA-AuNP nanovaccine at 5 weeks; macrophage inhibitors were prior to nanovaccine injection (n = 3 mice/group). The injected dose of 100 nm OVA-AuNP nanovaccine was normalized based on the injected OVA antigen amount (2.5 μg). Data shown as mean ± SD; *P < 0.05; **P < 0.01; ****P < 0.0001. All P values are from one-way ANOVA followed by Tukey's multiple comparisons tests.

if this approach of removing SCS macrophages can be applied for other vaccine formulations to boost their antibody production. We tested different vaccine formulations including antigen alone (Figure 3C) and antigen formulated with commercial adjuvant Alum (Figure 3D). Pretreatment using clodronate liposomes with these vaccine formulations showed significantly higher OVA-specific antibody production than PBS liposome pretreatment. We also found that nanovaccines

https://dx.doi.org/10.1021/acsnano.0c02240
ACS Nano XXXX, XXX, XXX–XXX

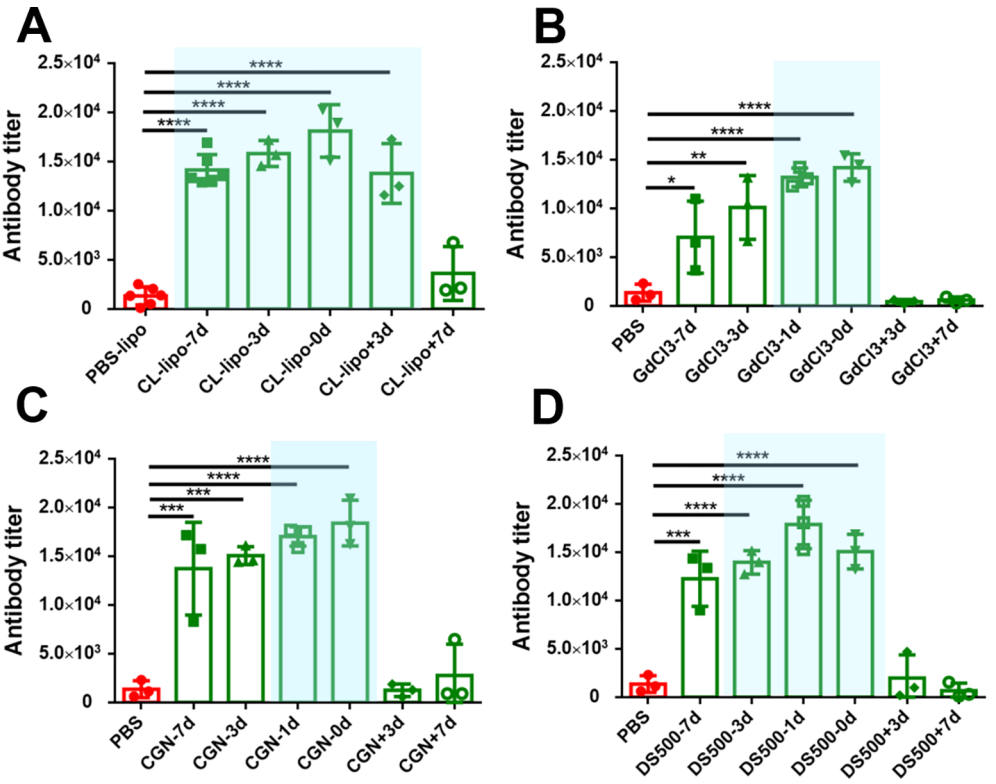

Figure 5. Assessing the administration windows of macrophage inhibitors for efficient OVA-specific antibody production. Antibody production at 5 weeks after (B) clodronate liposomes, (C) $GdCl_3$, (D) CGN, and (E) DS500 were intradermally footpad injected (7, 3, 1, and 0 days (3 h)) before or (3 and 7 days) after administration of 100 nm OVA-AuNP nanovaccine (n = 3−6 mice/group). The best administration windows were obtained for each macrophage inhibitor (blue shaded area) as determined by statistical comparison to the control PBS condition. Data shown as mean ± SD; *P < 0.05; **P < 0.01; ***P < 0.001; ****P < 0.0001. All P values are from one-way ANOVA followed by Tukey's multiple comparisons tests.

induce greater production of antigen-specific antibodies compared to free antigen and antigen formulated with the commercial adjuvant Alum in both PBS and clodronate liposomes pretreated conditions (Figure S8). We conclude that eliminating SCS macrophages is a universal approach to improving antigen-specific antibody production for a variety of vaccine designs.

Inhibition of Macrophage Uptake Function Improves Nanovaccine Delivery to Lymph Node Follicles and Induces Robust Humoral Immune Responses. We next determined if this phenomenon was clodronate liposome treatment-specific, or whether this phenomenon was related to the physical removal or functional removal of the SCS macrophages. SCS macrophages play key roles in innate immunity to protect the host against pathogens.[26] Repopulation of depleted SCS macrophages requires 2−6 months by monocytes.[23] It has been shown that chemical agents gadolinium chloride ($GdCl_3$), carrageenan (CGN), and dextran sulfate 500 (DS500) can inhibit macrophage uptake function (Figure S1).[29,32−38] We hypothesized that the pretreatment of the mice by these macrophage inhibitors can reduce the uptake capability of SCS macrophages without eliminating them. To test this hypothesis, we sacrificed the mice 24 h after intradermal footpad administration of various macrophage inhibitors, isolated sentinel lymph nodes for histological analysis, and then compared this to the PBS control. The injection doses of macrophage inhibitors were standardized to be 0.1 mg in a 20 μL volume. Histology revealed that SCS macrophages remained around the subcapsular sinus floor of lymph nodes 24 h after macrophage inhibitor pretreatment (Figure 4A), indicating that SCS macrophages were not eliminated after the pretreatment with macrophage inhibitors. CD169 (red color) was used to stain for SCS macrophages, and Prox1 (green color) was used to stain for LECs. We examined the TEM images with the enlarged panels focused on SCS macrophages after intradermal footpad injection of 100 nm OVA-AuNP nanovaccines after pretreatment of macrophage inhibitors (Figure 4B). SCS macrophages were labeled in green, and LECs were labeled in brown for better visualization. We found reduced amounts of 100 nm OVA-AuNP nanovaccines in SCS macrophages after all types of macrophage inhibitor pretreatment compared to PBS control. We conclude that the inhibition of macrophage uptake function is sufficient to reduce the OVA-AuNP nanovaccine sequestration by SCS macrophages in lymph nodes.

We then determined if pretreatment with macrophage inhibitors (i.e., agents that alter the uptake function) led to the same phenomenon as clodronate liposome pretreatment in mice, resulting in enhanced OVA-AuNP nanovaccine delivery to lymph node follicles and induction of robust humoral immune responses (Figure 4C−F). We sacrificed the mice 48 h after 100 nm OVA-AuNP nanovaccine administration following macrophage inhibitor pretreatment. We achieved 2 times enhanced OVA-AuNP nanovaccine accumulation in lymph node follicles after inhibition of macrophage function compared to PBS control (Figure 4C,E). Next, we immunized the mice using 100 nm OVA-AuNP nanovaccine (2.5 μg OVA

https://dx.doi.org/10.1021/acsnano.0c02240
ACS Nano XXXX, XXX, XXX−XXX

amount) after 24 h of macrophage inhibitor treatment and sacrificed the mice at 5 weeks. We achieved similar humoral immune responses across all macrophage inhibitor treatment groups (Figure 4D,F). We can induce germinal centers (red color) after all types of macrophage inhibitor pretreatment, but not in PBS control mice (Figure 4D). Mice pretreated with macrophage inhibitors had 10−13 times higher OVA-specific antibody production compared to PBS control (Figure 4F). Here, we explored the universality of macrophage inhibitors by disruption of SCS macrophage uptake, resulting in enhanced humoral immune responses.

Assessing the Administration Windows of Macrophage Inhibitors for Efficient Antibody Production. We next assessed the administration time windows of macrophage inhibitors for efficient antibody production (Figure 5A and Figure S9). Macrophage inhibitors can disrupt the SCS macrophage uptake function, but it is unclear how long this effect can last for OVA-AuNP nanovaccines. We asked the question: does the administration time between the macrophage inhibitor and OVA-AuNP nanovaccines influence the antigen-specific antibody production? We addressed this question by testing different time sequences between macrophage inhibitors and OVA-AuNP nanovaccine administration. Macrophage inhibitors (clodronate liposomes, $GdCl_3$, CGN, and DS500) were intradermally injected into the mouse footpad (7, 3, 1, and 0 days (3 h)) before or (3 and 7 days) after administration of 100 nm OVA-AuNP nanovaccines and compared to PBS control (Figure 5). We immunized the mice using 100 nm OVA-AuNP nanovaccines (2.5 μg OVA amount) and measured the OVA-specific antibody production from blood serum at 5 weeks. We found that the administration window to maximize antibody production is dependent on macrophage inhibitor type. They are highlighted using the blue shaded area in Figure 5. Clodronate liposomes deplete SCS macrophages and result in a broader window to induce efficient antibody production compared to PBS control. We failed to generate efficient antibody production when we administrated macrophage inhibitors 3−7 days after OVA-AuNP nanovaccine administration. We achieved efficient antibody production in all types of macrophage inhibitors when the macrophage inhibitors were administered 0−1 day prior to OVA-AuNP nanovaccines.

Macrophage Inhibitors Show Great Adjuvanticity When They Were Formulated with OVA-AuNP Nanovaccines. Vaccine formulations are typically formulated with antigens and adjuvants that are coadministrated. Adjuvants are used to amplify antigen-specific immune responses. Designing novel adjuvants enables us to better engineer the immune system and develop successful vaccines.[39−44] We found that pretreatment with macrophage inhibitors 0−1 day prior to OVA-AuNP nanovaccine administration resulted in enhanced antigen-specific antigen production (Figure 5); we proposed to formulate macrophage inhibitors with our 100 nm OVA-AuNP nanovaccines together to test the adjuvanticity of these macrophage inhibitors (Figure 6). We premixed the 100 nm OVA-AuNPs (2.5 μg OVA amount) with each macrophage inhibitor (0.1 mg) and injected them intradermally into the footpad of C57BL/6 mice. We measured the OVA-specific antibody production from blood serum at 1−5 weeks. We found that OVA-AuNP nanovaccines formulated with macrophage inhibitors induced greater OVA-specific antibody production than OVA-AuNP nanovaccines alone after 2 weeks of immunization. We also achieved 34−39 times higher

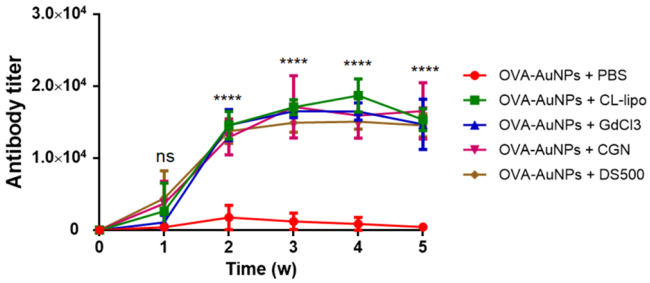

Figure 6. Macrophage inhibitors showed great adjuvanticity when they were formulated with OVA-AuNP nanovaccines. Antibody production after administration of OVA-AuNP nanovaccine and agents that inhibit macrophage uptake or deplete macrophages (n = 7 mice/group). The data were collected from two separate experiments. Data shown as mean ± SD; ns: not significant; ****P < 0.0001. All P values are from two-way ANOVA followed by Tukey's multiple comparisons tests.

OVA-specific antibody production immunized by OVA-AuNP nanovaccines formulated with different types of macrophage inhibitors compared to OVA-AuNP nanovaccines alone at 5 weeks (Figure 6). This finding is equivalent to the pretreatment with macrophage inhibitors (Figures 4H and 5B−E). We conclude that macrophage inhibitors can act as adjuvants that can be easily premixed with nanovaccines to induce greater humoral immune responses for more efficient vaccination.

Assessing the Toxicity of Macrophage Inhibitors. We finally tested the toxicity of these macrophage inhibitors. Macrophage inhibitors disrupt the SCS macrophage function of local lymph nodes after intradermal footpad administration. We asked the question "what are the consequences of local innate immunity suppression on mice, and could this induce systemic toxicity". We conducted a toxicology assessment using hematology and liver biochemistry assays. We injected the mice with 0.1 mg of these macrophage inhibitors and sacrificed the mice after 3 days. No significant difference in immune cell counts and hematological markers were determined across different macrophage inhibitors compared to PBS controls (Figures S10 and S11). We did not see any increase in all of the tested liver function biomarkers alanine aminotransferase (ALT), aspartate aminotransferase (AST), alkaline phosphatase (ALP), and total bilirubin (TBIL) after macrophage inhibitor treatment compared to PBS controls (Figure S12). All biomarker concentrations are within the normal range for C57BL/6 mice.[45] We did not observe systemic or gross inflammation in the histological sections of C57BL/6 mice hepatic tissue and splenic tissues after macrophage inhibitor treatment (Figures S13 and S14). It was also reported that macrophage depletion agents do not interfere with other immune cell populations in lymph nodes, such as CD4 and $\gamma\delta$ T cells, neutrophils, or dendritic cells.[24] Here, we conclude that this approach is safe because it only suppresses the SCS macrophage function and does not induce systemic toxicity.

CONCLUSIONS AND OUTLOOK

SCS macrophages are the first layer of defense in lymph nodes against pathogens and infectious disease.[31,46] These SCS macrophages are highly involved in the sequestration and clearance of viruses and bacteria. SCS macrophages can also capture viruses, bacteria, or immune complexes and promote antigen transport to B cell follicles to stimulate the humoral

https://dx.doi.org/10.1021/acsnano.0c02240
ACS Nano XXXX, XXX, XXX−XXX

immune responses.[2,12−17] However, the importance of SCS macrophages in promoting B cell-mediated humoral immunity has been recently challenged.[2,21,22,24] Here, we found that SCS macrophages play a barrier role to prevent OVA-AuNP nanovaccines from accessing lymph node follicles. Physical removal or functional impairment of SCS macrophages by chemical agents (clodronate liposomes, $GdCl_3$, CGN, or DS500) allowed OVA-AuNP nanovaccines to more efficiently deliver to and retain in follicles and interact with FDCs. This led to enhancement of humoral immune responses and eventually elicited up to 60 times more antigen-specific antibody production depending on nanovaccine design and injection dose. We summarized this finding with a schematic (Figure 7A). Our findings of greater B cell activation and

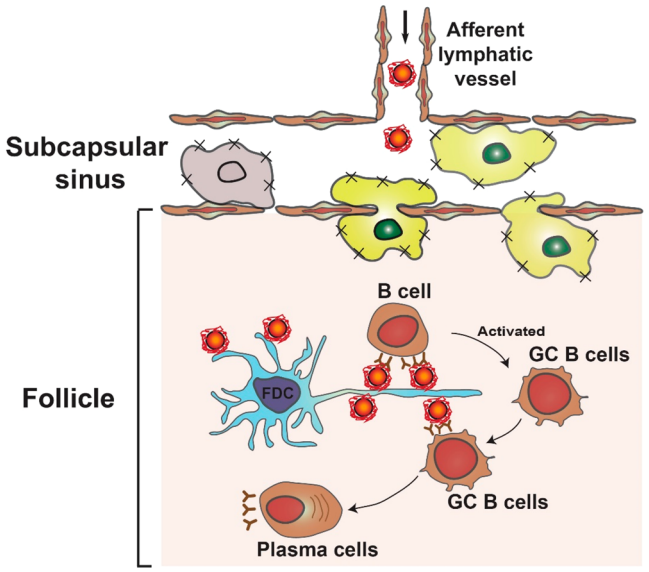

Figure 7. Schematic of transport of OVA-AuNP nanovaccines to the follicular dendritic cells in lymph node follicles for robust humoral immune responses. GC B cells are germinal center B cells.

antibody production after eliminating SCS macrophages using clodronate liposomes are supported by other groups.[21−26] It is worth mentioning that SCS macrophages are considered professional antigen presenting cells that directly activate T cells and natural killer T cells.[47−49] Depletion of SCS macrophages in tumor draining lymph nodes limits cancer cell clearance and promotes tumor growth.[26] This approach may be used to access the distant lymph nodes from a tumor that will not compromise T cell-mediated cellular immune responses against tumors.

We also tested other chemical agents, and they were not sufficient to remove macrophages or disrupt their uptake function and failed to generate enhanced OVA-AuNP nanovaccine follicle delivery and humoral immune responses. For example, clodronate needs to be encapsulated in a liposome formulation to induce macrophage depletion, whereas free clodronate agent alone (0.1 mg) cannot remove SCS macrophages and induce robust humoral immunity (Figure S15). Free clodronate formulated with OVA-AuNPs cannot induce effective vaccination compared to clodronate liposome formulated nanovaccines (Figure S16). Dextran sulfate 9 (DS9) (0.1 mg) (average molecular weight 9000−20 000 Da) is not sufficient to saturate macrophage scavenger receptors compared to DS500 (average molecular weight >500 000 Da) and failed to inhibit macrophage uptake function (Figure S17).[36] These results support the finding that inhibition of SCS macrophage uptake function is critical to allow more OVA-AuNP nanovaccines to enter lymph node follicles and mediate efficient humoral immune responses. The adjuvanticity of these macrophage inhibitor agents was determined by testing the neutralizing antibody production of immunized mice. The nanovaccines formulated with macrophage inhibitor agents resulted in more than 30 times higher antibody production compared to nanovaccines alone. This category of adjuvant shows the reverse effects of reducing innate immunity and boosting humoral immunity. We term them "reverse adjuvants". The mechanism of these adjuvants is different from any existing adjuvants used in vaccines.[39,40,43,50−55] The clinical applications of the "reverse adjuvants" need to be further explored in the future by combining with other commercially available adjuvants and vaccine formulations for specific infectious disease models. The potential adjuvanticity of other chemical agents for macrophage uptake inhibition including cell membrane, endocytosis, and cytoskeleton pathways needs to be evaluated in the future. This study demonstrates the role of SCS macrophages in the transport and delivery of nanovaccines to the lymph node follicle. Delivery to the final target in the lymph node is critical to the vaccines' ability to generate neutralizing antibodies.

MATERIALS AND METHODS

Synthesis of Gold Nanoparticles. Gold nanoparticles (AuNPs; 15 nm) were synthesized using a method adapted from Frens.[56] Briefly, 1 mL of 3% (w/v) sodium citrate tribasic (Sigma-Aldrich S4641) was prepared in 100 mL of deionized water and boiled. Under vigorous stirring, 100 μL of 10% (w/v) aqueous $HAuCl_4$ was added and allowed to react for 10 min. The reaction was then immediately cooled on ice to room temperature. These 15 nm AuNPs were then used for the preparation of 100 nm AuNPs as described previously by our group.[57] Molar equivalents of sodium citrate tribasic (1.5×10^{-2} M), aqueous $HAuCl_4$ (2.5×10^{-2} M), and 15 nm AuNPs ($2-4 \times 10^{-9}$ M) were added to 95−97 mL of deionized H_2O to make 100 mL total. The molar equivalent of hydroquinone (Sigma-Aldrich H17902) (2.5×10^{-2} M) was then added to the solution under vigorous stirring. The reaction was maintained overnight. Tween-20 (final concentration of 0.05% w/v) was added to the solution and stirred for 10 min. 100 nm AuNPs were then washed two times by centrifugation at 750*g*, resuspending the pellet in 0.02% sodium citrate tribasic and 0.05% Tween-20. AuNPs were stored at 4 °C for future use.

Synthesis of Nanoparticle Conjugated Vaccines (Nanovaccine). A model nanoparticle conjugated vaccine (nanovaccine) was composed of different sizes (15 and 100 nm) of AuNPs conjugated to ovalbumin (OVA) (Sigma-Aldrich A5503) antigen. AuNP stocks were washed once using 0.02% sodium citrate tribasic buffer for 35 min before OVA protein conjugation. 100 mM sodium citrate tribasic solution and HCl in deionized water was prepared, and pH was adjusted to 2.3. This solution was diluted to 20 mM of sodium citrate tribasic with approximately pH 3 and mixed with OVA into the final concentration of 10 mg/mL. OVA protein in 20 mM of sodium citrate tribasic was mixed on a rotator for 2 h and filtered using a 0.22 μm PES filter. 250 μL of OVA solution was added in to the AuNP solution with 1.6×10^{16} nm^2 total surface area. The mixed solution was then incubated in a 1.5 mL Eppendorf tube at 37 °C for 1 h. After conjugation, the mixed solution was topped up with 1× PBS + 0.05% Tween-20. The OVA conjugated AuNPs (OVA-AuNPs) were then wash with 1× PBS + 0.05% Tween-20 and purified with centrifugation speeds of 5000*g* for 15 nm AuNPs and 200*g* for 100 nm AuNPs for 60 min. OVA-AuNPs were purified three times and resuspended in sterile PBS. OVA-AuNP nanovaccine was filtered

https://dx.doi.org/10.1021/acsnano.0c02240
ACS Nano XXXX, XXX, XXX−XXX

using a 0.22 μm PES filter to remove the possible aggregates. The OVA-AuNP nanovaccine concentration was justified before footpad intradermal injection.

Physicochemical Characterization of Gold Nanoparticles and Nanovaccines. The core sizes of AuNPs and OVA-AuNPs were characterized by transmission electron microscopy (TEM) (Figure S4 and Table S1). TEM copper grids (Ted Pella 01813-F) were plasma treated. AuNP or OVA-AuNP nanovaccine stock (5 μL) was added on the treated TEM grids. The samples were blotted after 3 min using Kimwipes. The samples were left on grids for another 10 min to be completely air-dried. OVA-AuNP samples on the EM grid were washed one more time with 5 μL of deionized water and blotted using Kimwipes. The samples were negatively stained with 3 μL of 1% uranyl acetate (Ted Pella 19481). The stained samples were blotted using Kimwipes after 1 min of staining and air-dried for 10 more minutes. All samples were visualized using TEM at 120 kV (Tecnai 20, FEI, Hillsboro, OR) with an AMT 16000 camera. The AuNP core sizes were analyzed using ImageJ (NIH, Maryland).[58] The hydrodynamic diameters were characterized using dynamic light scattering (DLS) (Malvern Instruments Ltd., Worcestershire, UK), and absorbance was measured using UV−vis absorbance spectroscopy (Shimadzu Scientific Instruments). The surface charge was measured using a Zetasizer Nano-ZS (Malvern Instruments Ltd.) instrument in 150 mM HEPES, pH 7.5. The concentrations of AuNPs and OVA-AuNP were measured using UV−vis absorbance spectroscopy. The amount of OVA protein conjugated on AuNP was measured by bicinchoninic acid (BCA) assay (ThermoFisher Scientific 23235).

Extraction and Quantification of OVA Protein Using Bicinchoninic Acid Assay. OVA-AuNP nanovaccine solution with 2×10^{14} nm^2 total surface area was resuspended in 25 μL of PBS in a 1.5 mL Eppendorf tube. 4% NuPAGE LDS buffer (8 μL, ThermoFisher Scientific NP0007) and 4 μL of 500 mM dithiothreitol (DTT) (BioShop DTT001.5) were mixed with OVA-AuNP solution in the Eppendorf. This solution was then incubated at 70 °C for 1 h. The Eppendorf was centrifuged at 18 000g for 15 min. The supernatant was collected and mixed with 25 μL of 2% (w/v) sodium dodecyl sulfate (SDS) (ThermoFisher Scientific NP0001). To eliminate the SDS and DTT from the isolated OVA protein, 950 μL of 10% (w/v) trichloroacetic acid (TCA) (Sigma-Aldrich T6399) in acetone was added into the Eppendorf tube and incubated at −80 °C for 12 h. The Eppendorf tube was centrifuged at 18 000g at 4 °C for 15 min. The supernatant was removed, and the OVA protein was resuspended in 500 μL of 0.03% (w/v) deoxycholate (Sigma-Aldrich 30970) and vortexed thoroughly. 100 μL of 72% (w/v) TCA was mixed into the Eppendorf and incubated on ice for 30 min. The protein was centrifuged at 18 000g at 4 °C for 15 min. 950 μL of acetone (−30 °C) was mixed into the Eppendorf tube and vortexed thoroughly. The tube was incubated at −80 °C for 1 h. The isolated OVA protein was pelleted at the bottom after centrifugation at 18 000g at 4 °C for 15 min. The supernatant was removed, and the isolated protein was air-dried for 30 min. The purified protein was dissolved into a 2% (w/v) SDS solution in PBS. To establish the standard curve, OVA protein was dissolved into a 2% (w/v) SDS solution in PBS and diluted stepwise. The purified protein and standards were incubated at 70 °C for 1 h. 200 μL of the bicinchoninic acid (BCA) (Thermo Fisher Scientific 23235) reagent I from the kit was added to all samples and standards. These samples and standards were incubated at 60 °C for 30 min until a purple color developed. All samples and standards were cooled to room temperature and analyzed on an absorbance plate reader at 562 nm (Tecan Sunrise). The protein amount was calculated based on the standard curve. The injected OVA-AuNP dose is normalized based on the injected OVA antigen amount (10 μg) (Figure S5).

Animal Care. Mice studies were performed under the restriction and protocols at the University of Toronto Division of Comparative Medicine (protocol numbers: 20011620, 20011910, 20012102). Wild-type C57BL/6 mice (8−12 weeks old) were purchased form Charles River Laboratories (Montreal, Canada). Mice were anesthetized under isoflurane (3%) carried with oxygen during intradermal footpad injection. OVA-AuNP nanovaccines were intradermally injected using a 29-gauge insulin needle. The injected dose was normalized to the OVA protein amount. The injected volume was 20 μL for each footpad. Four footpads were injected in each mouse. The axillary, brachial, and popliteal sentinel lymph nodes were collected for further studies.

Administration of Macrophage Inhibitors. Clodronate or PBS liposomes (Liposoma BV CP-005-005) were used to eliminate subcapsular sinus (SCS) macrophages in lymph nodes (Figure S1). Other macrophage inhibitors including gadolinium chloride ($GdCl_3$) (Sigma-Aldrich 203289), carrageenan (CGN) (Sigma-Aldrich C1138), and dextran sulfate 500 (DS500) (Sigma-Aldrich D6001) were used to inhibit SCS macrophage uptake function (Figure S1). Free clodronate (clodronic acid disodium salt hydrate) (TRC Canada C586875) and low-molecular-weight dextran sulfate 9 (DS9) (average molecular weight 9000−20 000 Da) (Sigma-Aldrich D6924) were used as negative controls, which cannot effectively physically or functionally eliminate macrophages. Macrophage inhibitors (20 μL) were intradermally injected into the footpads of C57BL/6 mice using 29-gauge insulin syringes. Equivalently, the amount of injected macrophage inhibitors was 0.1 mg per footpad, in total 0.4 mg for four footpads. Macrophage inhibitors were intradermally injected into the mouse footpad (7, 3, 1, and 0 days (3 h)) before or (3 and 7 days) after administration of 100 nm OVA-AuNP nanovaccine.

Histology, Antibody Staining, and Imaging. The axillary, brachial, and popliteal sentinel lymph nodes were collected for histological analysis after 2 h to 5 weeks injection. The collected sentinel lymph nodes were frozen using liquid nitrogen in a frozen section compound solution (VWR International, LLC 95057-838) in a plastic cryomold (Tissue-Tek at VWR 4565). This method can preserve the antigens on cell membrane for immunostaining. The frozen histology samples were processed at the Toronto Centre for Phenogenomics (TCP). Sample sections (8 μm) were cut on Cryostar NX70 and placed on charged slides. To visualize OVA-AuNP distribution, sample sections were stained using silver enhancement kits (Ted Pella, Inc. 15718) for enhancement of the gold signal. Prior to the immunostaining, sample sections were fixed in 10% neutral buffered formalin, permeabilized in 0.5% Triton X-100. All sections were incubated in primary antibody overnight at 4 °C, rinsed in TBST, and then incubated in secondary antibody for 1 h at room temperature. The subcapsular sinus (SCS) macrophages were stained using rat antisialoadhesin (CD169) antibody (Abcam ab53443; 1:600) followed by antirat secondary conjugated with Alexa Fluor 488 (Abcam ab150165; 1:200). Lymphatic endothelial cells were labeled using rabbit anti-Lyve1 antibody (Abcam ab14917; 1:500) followed by antirabbit secondary conjugated with Alexa Fluor 555 (Thermo Fisher A21428; 1:200), Syrian hamster antipodoplanin antibody (BioXCell BE0236; 1:1000) followed by biotinylated anti-Syrian Hamster IgG (Abcam ab6891; 1:200), and then Streptavidin-Alexa Fluor 594 (Thermo Fisher S11227; 1:1000) or rabbit anti-Prox1 antibody (BioLegend 925201; 1:1500) followed by antirabbit secondary conjugated with Alexa Fluor 555. Follicular dendritic cells (FDCs) were labeled using rabbit anti-CD21 antibody (Abcam ab75985; 1:1800) followed by antirabbit secondary conjugated with Alexa Fluor 555. B cells were detected using rat anti-B220 antibody (eBioscience 14-0452-82; 1:100) followed by antirat secondary conjugated with Alexa Fluor 674 (ThermoFisher A21247; 1:200). Germinal center formation was labeled using rat anti-GL7 antibody (FITC) (BioLegend 144604; 1:250). Nuclei were then counter-stained with DAPI (Sigma-Aldrich D9542) on sample sections. The sample sections were scanned using an Olympus VS-120 slide scanner and imaged using a Hamamatsu ORCA-R2 C10600 digital camera for all bright-field and fluorescent images. The images of silver stained OVA-AuNPs in lymph node follicles were analyzed using ImageJ (NIH).[58] The spaces between lymphatic endothelial cells were measured using ImageJ (NIH).[58]

TEM Study on Lymph Node Tissues. SCS macrophage location, sinus structure, FDCs in lymph node follicles, and the location of OVA-AuNPs were studied using TEM at the subcellular level. The mice were sacrificed after different injection times (12 or 48 h). The axillary, brachial, and popliteal sentinel lymph nodes were collected

https://dx.doi.org/10.1021/acsnano.0c02240
ACS Nano XXXX, XXX, XXX−XXX

and fixed with 4% formaldehyde and 0.5% glutaraldehyde (Sigma-Aldrich 340855) in PBS at room temperature for 1 h. The samples were stored at 4 °C. The fixed samples were processed at the Nanoscale Biomedical Imaging Facility at The Hospital for Sick Children. The lymph node samples were sectioned and placed on copper grids (Ted Pella 01813-F). The sectioned tissue samples were negative stained with 2% uranyl acetate (Ted Pella 19481) on copper grids. The images were taken using TEM at 120 kV. The spaces between lymphatic endothelial cells were measured using ImageJ (NIH).[58] The numbers of nanovaccines on FDC dendrites were quantified using TEM images. The numbers of 100 nm OVA-AuNP nanovaccines per the area (um^2) of FDC dendrites were calculated.

Lymph Node Disaggregation, Cell Staining, and Flow Cytometry. The percentage of germinal center B cells ($GL7^+B220^+$) and number of germinal center B cells ($GL7^+B220^+$) were studied using flow cytometry. The mice were sacrificed after 5 weeks of immunization. The axillary, brachial, and popliteal sentinel lymph nodes were collected and mechanically disaggregated. These lymph node samples were then placed into the preprepared enzyme digestion solution in an Eppendorf tube. This solution contains 958 μL of Hanks' balanced salt solution (HBSS) buffer (ThermoFisher Scientific 14185052), 40 μL of 10 mg/mL collagenase IV (Sigma-Aldrich C5138), and 2 μL of 10 mg/mL of DNase (Roche 10104159001). Lymph node samples were incubated at 37 °C for 30 min. The samples were filtered through a 70 μm cell strainer. Lymph node cells were pellet down at 300*g* at 4 °C for 10 min in an Eppendorf tube. The isolated cells were resuspended in HBSS blocking buffer contained with 0.5% (w/v) bovine serum albumin and 2 mM EDTA. The Fc receptor was blocked using Anti-CD16/32 antibody (BioLegend 101302) for 30 min on ice. Cocktail antibodies, Zombie NIR live/dead stain (BioLegend 423106), BV510 anti-B220 (RA3-6B2) (BioLegend 103247), and Alexa Fluor 647 anti-GL7 (BioLegend 144606) were then mixed with the samples and placed on ice for 30 min. The samples were washed by HBSS blocking buffer after antibody staining. The samples were fixed using 1.6% paraformaldehyde (Thermo Fisher Scientific 28906) in HBSS on ice for 30 min. The samples were placed in HBSS blocking buffer for further flow cytometry study. The events were acquired by a 5-laser BD LSR FORTESSA X-20 flow cytometer. The flow data were processed by FlowJo V10 software.

ELISA of OVA-Specific Antibody Production. Mice were sacrificed after 1−5 weeks of immunization. OVA-specific antibody production was measured in the blood sera using enzyme-linked immunosorbent assay (ELISA). A 20 μg/mL concentration of OVA in PBS solution was preprepared. A 100 μL portion of OVA solution was coated on a MaxiSorp 96-well plate (Thermo Fisher Scientific 442404) at 4 °C overnight. The solution was removed. The wells were washed once with 400 μL of PBST. 200 μL of 1× casein buffer (Sigma-Aldrich B6429-500 ML) was added into each well at room temperature for 2 h. The plate was washed once with 400 μL of PBST. The blood serum samples were diluted 100 times with 0.5× Casein buffer and added into the first lane of the plate (200 μL). 100 μL of 0.5× casein buffer was added into the other lanes with the serial dilution of the blood sera until the second final lane. The last lane was kept a baseline. All samples were placed at room temperature for 1 h. The plate was washed two times using PBST (400 μL). Goat antimouse IgG secondary antibody and horseradish peroxidase (HRP) (Thermo Fisher Scientific 31430) were diluted 5000 times and added into each well (100 μL). All samples were placed at room temperature for 1 h. The plate was washed two times using PBST (400 μL). TMB (3,3′,5,5;-tetramethylbenzidine) chromogen solution (Thermo Fisher Scientific 002023) was added into each well (100 μL). The plate was placed at room temperature for 10 min until the blue color developed. Sulfuric acid (1 M; 100 μL) was added into each well (100 μL). The absorbance was acquired using an absorbance plate reader (Tecan Sunrise) at 450 nm. The reference was at 570 nm. All titers were determined as inverse dilutions where $A_{450nm} - A_{570nm}$ equals 0.1.

Toxicity Evaluation of Macrophage Inhibitors. Toxicology assessments of macrophage inhibitors were conducted using hematology and liver biochemistry assays. Macrophage inhibitors of clodronate liposomes, $GdCl_3$, CGN, and DS500 were intradermally injected into the mouse footpad. The amount of injected macrophage inhibitors was 0.1 mg per footpad, in total 0.4 mg for four footpads. Mice were sacrificed after 3 days of injection. Blood samples were collected through cardiac puncture using a 23-gauge needle and separated into two fractions. One fraction of blood was transferred to microfuge tubes containing dipotassium EDTA and kept on ice. These samples were taken to the DCM of Medical Science Building at the University of Toronto on ice for immune cell analysis and hematology analysis. The immune cell included white blood cells, lymphocytes, monocytes, and neutrophils. Hematology analysis included red blood cell (RBC), hemoglobin (HGB), hematocrit (HCT), mean corpuscular volume (MCV), mean corpuscular hemoglobin (MCH), mean corpuscular hemoglobin concentration (MCHC), platelet (PLT), mean platelet volume (MPV), and platelet hematocrit (%). The other blood fraction was centrifuged down at 500*g* for 10 min, and the blood sera was collected. The sera samples were taken to the Toronto Centre for Phenogenomics (TCP) on dry ice for hepatotoxicity analysis of serum markers. Serum markers of liver parenchyma included alanine transaminase (ALT), aspartate aminotransferase (AST), alkaline phosphatase (ALP), and total bilirubin (TBIL). Liver and spleen sections were cut and fixed in 10% formalin for 1 day. The fixed tissue sections were taken to Toronto Centre for Phenogenomics (TCP) for further sample processing. Liver and spleen tissue sections were stained with hematoxylin and eosin to observe any systemic or gross inflammation. The sample sections were scanned using an Olympus VS-120 slide scanner and imaged using a Hamamatsu ORCA-R2 C10600 digital camera for all bright-field images.

Statistical Analysis. Data were collected from 3−7 mice per group. All statistical analysis was performed using GraphPad Prism 6.0. Analyzed data were performed using one-way or two-way ANOVA followed by Tukey's multiple comparisons test or an unpaired *t* test. All data were shown as mean ± SD; statistical significance was determined as ns: not significant; $*P < 0.05$; $**P < 0.01$; $***P < 0.001$; $****P < 0.0001$.

ASSOCIATED CONTENT

Supporting Information

The Supporting Information is available free of charge at https://pubs.acs.org/doi/10.1021/acsnano.0c02240.

Mechanism of macrophage inhibitors, quantification of space between lymphatic endothelial cells, nanoparticle and nanovaccine characterization, quantification of antigen protein amount on AuNPs, more representative TEM images of subcapsular sinus macrophages and follicular dendritic cells, gating strategy for flow cytometry, toxicity evaluation of macrophage inhibitors, and free clodronate and DS9 (average molecular weight 9000−20 000 Da) that are not sufficient to inhibit macrophage function (PDF)

AUTHOR INFORMATION

Corresponding Author

Warren C.W. Chan − *Institute of Biomaterials & Biomedical Engineering, Terrence Donnelly Centre for Cellular & Biomolecular Research, Department of Chemical Engineering & Applied Chemistry, Department of Materials Science & Engineering, and Department of Chemistry, University of Toronto, Toronto, Ontario M5S 3G9, Canada;* orcid.org/0000-0001-5435-4785; Email: warren.chan@utoronto.ca

Authors

Yi-Nan Zhang − *Institute of Biomaterials & Biomedical Engineering and Terrence Donnelly Centre for Cellular &*

https://dx.doi.org/10.1021/acsnano.0c02240
ACS Nano XXXX, XXX, XXX−XXX

Biomolecular Research, University of Toronto, Toronto, Ontario M5S 3G9, Canada

Wilson Poon − *Institute of Biomaterials & Biomedical Engineering and Terrence Donnelly Centre for Cellular & Biomolecular Research, University of Toronto, Toronto, Ontario M5S 3G9, Canada*

Elana Sefton − *Institute of Biomaterials & Biomedical Engineering and Terrence Donnelly Centre for Cellular & Biomolecular Research, University of Toronto, Toronto, Ontario M5S 3G9, Canada*

Complete contact information is available at: https://pubs.acs.org/10.1021/acsnano.0c02240

Author Contributions

Y.-N.Z. and W.C.W.C. conceptualized the project. Y.-N.Z. and E.S. designed, synthesized, and characterized nanoparticles and nanovaccines. Y.-N.Z., W.P., and E.S. designed, performed, and analyzed experiments. Y.-N.Z. and W.C.W.C. wrote the initial manuscript draft. All authors contributed to review and editing of the manuscript.

Notes

The authors declare no competing financial interest.

Data and materials availability: all data are available in the main text or the Supporting Information.

ACKNOWLEDGMENTS

We acknowledge A.J. Tavares, L.N.M. Nguyen, and F. Song from our lab for fruitful discussions. Y.-N.Z. thanks Z. Hao at The Donnelly Centre for Cellular and Biomolecular Research of University of Toronto for valuable suggestion and discussion on humoral function tests. We thank A. Darbandi and D. Holmyard at The Hospital for Sick Children Nanoscale Biomedical Imaging Facility for TEM sample preparation and their expertise in TEM operation. We thank V. Bradaschia and M. Ganguly at the Toronto Centre for Phenogenomics for their expertise in histology and immunostaining. We thank D. White and J. Warzyszynska at Faculty of Medicine Flow Cytometry Facility of Univeristy of Toronto for their expertise in flow cytometry. This study was supported by Canadian Cancer Society Research Institute, Canadian Institutes of Health Research (CIHR) Grant MOP-130143, Natural Sciences and Engineering Research Council of Canada (NSERC) Grant 2015-06397, and a Collaborative Health Research Project (CHRP-493619-16). Y.-N.Z. thanks NSERC, OGS, Wildcat Foundation, and Paul and Sally Wang for provision of fellowships and graduate scholarships. W.P. thanks CIHR, OGS, Barbara and Frank Milligan, and Cecil Yip for provision of fellowships and graduate scholarships. Last but not least, Y.-N.Z. thanks his family for their continuous supports during this project, to his grandma F.P. Zhu, father Q. Zhang, father-in-law Y.H. Gao, and especially to his wife B. Gao.

REFERENCES

(1) Rappuoli, R. Glycoconjugate Vaccines: Principles and Mechanisms. *Sci. Transl. Med.* **2018**, *10*, No. eaat4615.

(2) Cyster, J. G. B. Cell Follicles and Antigen Encounters of the Third Kind. *Nat. Immunol.* **2010**, *11*, 989−996.

(3) Victora, G. D.; Nussenzweig, M. C. Germinal Centers. *Annu. Rev. Immunol.* **2012**, *30*, 429−457.

(4) Sun, X.; Stefanetti, G.; Berti, F.; Kasper, D. L. Polysaccharide Structure Dictates Mechanism of Adaptive Immune Response to Glycoconjugate Vaccines. *Proc. Natl. Acad. Sci. U. S. A.* **2019**, *116*, 193−198.

(5) Allen, C. D. C.; Okada, T.; Cyster, J. G. Germinal-Center Organization and Cellular Dynamics. *Immunity* **2007**, *27*, 190−202.

(6) Cyster, J. G.; Allen, C. D. C. B Cell Responses: Cell Interaction Dynamics and Decisions. *Cell* **2019**, *177*, 524−540.

(7) Heesters, B. A.; van der Poel, C. E.; Das, A.; Carroll, M. C. Antigen Presentation to B Cells. *Trends Immunol.* **2016**, *37*, 844−854.

(8) De Silva, N. S.; Klein, U. Dynamics of B cells in Germinal Centres. *Nat. Rev. Immunol.* **2015**, *15*, 137−148.

(9) Rantakari, P.; Auvinen, K.; Jäppinen, N.; Kapraali, M.; Valtonen, J.; Karikoski, M.; Gerke, H.; Iftakhar-E-Khuda, I.; Keuschnigg, J.; Umemoto, E.; Tohya, K.; Miyasaka, M.; Elima, K.; Jalkanen, S.; Salmi, M. The Endothelial Protein PLVAP in Lymphatics Controls the Entry of Lymphocytes and Antigens into Lymph Nodes. *Nat. Immunol.* **2015**, *16*, 386−396.

(10) Hons, M.; Sixt, M. The Lymph Node Filter Revealed. *Nat. Immunol.* **2015**, *16*, 338−340.

(11) Roozendaal, R.; Mempel, T. R.; Pitcher, L. A.; Gonzalez, S. F.; Verschoor, A.; Mebius, R. E.; von Andrian, U. H.; Carroll, M. C. Conduits Mediate Transport of Low-Molecular-Weight Antigen to Lymph Node Follicles. *Immunity* **2009**, *30*, 264−276.

(12) Phan, T. G.; Green, J. A.; Gray, E. E.; Xu, Y.; Cyster, J. G. Immune Complex Relay by Subcapsular Sinus Macrophages and Noncognate B Cells Drives Antibody Affinity Maturation. *Nat. Immunol.* **2009**, *10*, 786−793.

(13) Phan, T. G.; Grigorova, I.; Okada, T.; Cyster, J. G. Subcapsular Encounter and Complement-Dependent Transport of Immune Complexes by Lymph Node B Cells. *Nat. Immunol.* **2007**, *8*, 992−1000.

(14) Junt, T.; Moseman, E. A.; Iannacone, M.; Massberg, S.; Lang, P. A.; Boes, M.; Fink, K.; Henrickson, S. E.; Shayakhmetov, D. M.; Di Paolo, N. C.; van Rooijen, N.; Mempel, T. R.; Whelan, S. P.; von Andrian, U. H. Subcapsular Sinus Macrophages in Lymph Nodes Clear Lymph-Borne Viruses and Present Them to Antiviral B Cells. *Nature* **2007**, *450*, 110−114.

(15) Gonzalez, S. F.; Degn, S. E.; Pitcher, L. A.; Woodruff, M.; Heesters, B. A.; Carroll, M. C. Trafficking of B cell Antigen in Lymph Nodes. *Annu. Rev. Immunol.* **2011**, *29*, 215−233.

(16) Kuka, M.; Iannacone, M. Viral Subversion of B Cell Responses Within Secondary Lymphoid Organs. *Nat. Rev. Immunol.* **2018**, *18*, 255−265.

(17) Carrasco, Y. R.; Batista, F. D. B. Cells Acquire Particulate Antigen in a Macrophage-Rich Area at the Boundary Between the Follicle and the Subcapsular Sinus of the Lymph Node. *Immunity* **2007**, *27*, 160−171.

(18) Heesters, B. A.; Myers, R. C.; Carroll, M. C. Follicular Dendritic Cells: Dynamic Antigen Libraries. *Nat. Rev. Immunol.* **2014**, *14*, 495−504.

(19) Kratzer, R.; Mauvais, F.-X.; Burgevin, A.; Barilleau, É.; van Endert, P. Fusion Proteins for Versatile Antigen Responses Differential Capacity to Prime Immune Targeting to Cell Surface Receptors Reveal Differential Capacity to Prime Immune Responses. *J. Immunol.* **2010**, *184*, 6855−6864.

(20) Taylor, P. R.; Zamze, S.; Stillion, R. J.; Wong, S. Y. C.; Gordon, S.; Martinez-Pomares, L. Development of A Specific System for Targeting Protein to Metallophilic Macrophages. *Proc. Natl. Acad. Sci. U. S. A.* **2004**, *101*, 1963−1968.

(21) Gonzalez, S. F; Lukacs-Kornek, V.; Kuligowski, M. P; Pitcher, L. A; Degn, S. E.; Kim, Y.-A; Cloninger, M. J; Martinez-Pomares, L.; Gordon, S.; Turley, S. J; Carroll, M. C Capture of Influenza by Medullary Dendritic Cells *via* SIGN-R1 is Essential for Humoral Immunity in Draining Lymph Nodes. *Nat. Immunol.* **2010**, *11*, 427−434.

(22) Iannacone, M.; Moseman, E. A.; Tonti, E.; Bosurgi, L.; Junt, T.; Henrickson, S. E.; Whelan, S. P.; Guidotti, L. G.; von Andrian, U. H. Subcapsular Sinus Macrophages Prevent CNS Invasion on Peripheral Infection with A Neurotropic Virus. *Nature* **2010**, *465*, 1079−1083.

(23) Delemarre, F. G.A.; Kors, N.; van Rooijen, N. The *In Situ* Immune Response in Popliteal Lymph Nodes of Mice after Macrophage Depletion. Differential Effects of Macrophages on

Thymus-Dependent and Thymus-Independent Immune Responses. *Immunobiology* **1990**, *180*, 395−404.
(24) Tonti, E.; Jiménez de Oya, N.; Galliverti, G.; Moseman, E. A.; Di Lucia, P.; Amabile, A.; Sammicheli, S.; Giovanni, M. de; Sironi, L.; Chevrier, N.; Sitia, G.; Gennari, L.; Guidotti, L. G.; von Andrian, U. H.; Iannacone, M. Bisphosphonates Target B Cells to Enhance Humoral Immune Responses. *Cell Rep.* **2013**, *5*, 323−330.
(25) Farrell, H. E.; Davis-Poynter, N.; Bruce, K.; Lawler, C.; Dolken, L.; Mach, M.; Stevenson, P. G. Lymph Node Macrophages Restrict Murine Cytomegalovirus Dissemination. *J. Virol.* **2015**, *89*, 7147−7158.
(26) Pucci, F.; Garris, C.; Lai, C. P.; Newton, A.; Pfirschke, C.; Engblom, C.; Alvarez, D.; Sprachman, M.; Evavold, C.; Magnuson, A.; von Andrian, U. H.; Glatz, K.; Breakefield, X. O.; Mempel, T. R.; Weissleder, R.; Pittet, M. J. SCS Macrophages Suppress Melanoma by Restricting Tumor-Derived Vesicle-B Cell Interactions. *Science* **2016**, *352*, 242−246.
(27) Delemarre, F. G. A.; Kors, N.; Kraal, G.; van Rooijen, N. Repopulation of Macrophages in Popliteal Lymph Nodes of Mice After Liposome-mediated Depletion. *J. Leukocyte Biol.* **1990**, *47*, 251−257.
(28) Oussoren, C.; Velinova, M.; Scherphof, G.; van der Want, J. J.; van Rooijen, N.; Storm, G. Lymphatic Uptake and Biodistribution of Liposomes After Subcutaneous Injection IV. Fate of Liposomes in Regional Lymph Nodes. *Biochim. Biophys. Acta, Biomembr.* **1998**, *1370*, 259−272.
(29) van Rooijen, N.; Sanders, A. Elimination, Blocking, and Activation of Macrophages: Three of a Kind? *J. Leukocyte Biol.* **1997**, *62*, 702−709.
(30) Zhang, Y.-N.; Lazarovits, J.; Poon, W.; Ouyang, B.; Nguyen, L. N. M.; Kingston, B. R.; Chan, W. C. W. Nanoparticle Size Influences Antigen Retention and Presentation in Lymph Node Follicles for Humoral Immunity. *Nano Lett.* **2019**, *19*, 7226−7235.
(31) Louie, D. A. P.; Liao, S. Lymph Node Subcapsular Sinus Macrophages as the Frontline of Lymphatic Immune Defense. *Front. Immunol.* **2019**, *10*, 347.
(32) Zhang, Y.-N.; Poon, W.; Tavares, A. J.; McGilvray, I. D.; Chan, W. C. W. Nanoparticle-Liver Interactions: Cellular Uptake and Hepatobiliary Elimination. *J. Controlled Release* **2016**, *240*, 332−348.
(33) Diagaradjane, P.; Deorukhkar, A.; Gelovani, J. G.; Maru, D. M.; Krishnan, S. Gadolinium Chloride Augments Tumor-Specific Imaging of Targeted Quantum Dots *In Vivo*. *ACS Nano* **2010**, *4*, 4131−4141.
(34) Fowler, E. F.; Thomson, A. W. Effect of Carrageenan on Activity of the Mononuclear Phagocyte System in the Mouse. *Br. J. Exp. Pathol.* **1978**, *59*, 213−219.
(35) Nicklin, S.; Atkinson, H.; Miller, K. Iota-Carrageenan Induced Reaginic Antibody Production in the Rat-I. Characterisation and Kinetics of the Response. *Int. J. Immunopharmacol.* **1985**, *7*, 677−685.
(36) Bradfield, J. W. B.; Souhami, R. L.; Addison, I. E. The Mechanism of the Adjuvant Effect of Dextran Sulphate. *Immunology* **1974**, *26*, 383−392.
(37) Kamochi, M.; Ogata, M.; Yoshida, S.; Matsumoto, T.; Kubota, E.; Mizuguchi, Y.; Shigematsu, A. Dextran Sulphate Enhancement of Lipopolysaccharide-Induced Tumour Necrosis Factor-α Production by Murine Peritoneal Macrophages: Correlation with Macrophage Blockade. *FEMS Immunol. Med. Microbiol.* **1993**, *7*, 153−159.
(38) Rüttinger, D.; Vollmar, B.; Wanner, G. A.; Messmer, K. *In Vivo* Assessment of Hepatic Alterations Following Gadolinium Chloride-Induced Kupffer Cell Blockade. *J. Hepatol.* **1996**, *25*, 960−967.
(39) Rappuoli, R. Rino Rappuoli. *Nat. Rev. Drug Discovery* **2007**, *6*, 694.
(40) Rappuoli, R. Bridging the Knowledge Gaps in Vaccine Design. *Nat. Biotechnol.* **2007**, *25*, 1361−1366.
(41) Delany, I.; Rappuoli, R.; Gregorio, E. de. Vaccines for the 21st Century. *EMBO Mol. Med.* **2014**, *6*, 708−720.
(42) Del Giudice, G.; Podda, A.; Rappuoli, R. What are the Limits of Adjuvanticity? *Vaccine* **2001**, *20*, S38−41.
(43) Reed, S. G.; Orr, M. T.; Fox, C. B. Key Roles of Adjuvants in Modern Vaccines. *Nat. Med.* **2013**, *19*, 1597−1608.
(44) Rappuoli, R.; Aderem, A. A. 2020 Vision for Vaccines against HIV, Tuberculosis and Malaria. *Nature* **2011**, *473*, 463−469.
(45) Charles River. *Biochemistry and Hematology for C57BL/6NCrl Mouse Colonies in North America for January 2008 − December 2012*. https://www.criver.com/sites/default/files/Technical%20Resources/Biochemistry%20and%20Hematology%20for%20C57BL_6NCrl%20Mouse%20Colonies%20in%20North%20American%20for%20January%202008%20%E2%80%93%20December%202012.pdf (accessed November 15, 2019).
(46) Moran, I.; Grootveld, A. K.; Nguyen, A.; Phan, T. G. Subcapsular Sinus Macrophages: The Seat of Innate and Adaptive Memory in Murine Lymph Nodes. *Trends Immunol.* **2019**, *40*, 35−48.
(47) Asano, K.; Nabeyama, A.; Miyake, Y.; Qiu, C.-H.; Kurita, A.; Tomura, M.; Kanagawa, O.; Fujii, S.-i.; Tanaka, M. CD169-Positive Macrophages Dominate Antitumor Immunity by Crosspresenting Dead Cell-Associated Antigens. *Immunity* **2011**, *34*, 85−95.
(48) Barral, P.; Polzella, P.; Bruckbauer, A.; van Rooijen, N.; Besra, G. S.; Cerundolo, V.; Batista, F. D. CD169(+) Macrophages Present Lipid Antigens to Mediate Early Activation of iNKT Cells in Lymph Nodes. *Nat. Immunol.* **2010**, *11*, 303−312.
(49) Bernhard, C. A.; Ried, C.; Kochanek, S.; Brocker, T. CD169+ Macrophages Are Sufficient for Priming of CTLs with Specificities Left Out by Cross-Priming Dendritic Cells. *Proc. Natl. Acad. Sci. U. S. A.* **2015**, *112*, 5461−5466.
(50) Moyer, T. J.; Zmolek, A. C.; Irvine, D. J. Beyond Antigens and Adjuvants: Formulating Future Vaccines. *J. Clin. Invest.* **2016**, *126*, 799−808.
(51) Pulendran, B.; Ahmed, R. Immunological Mechanisms of Vaccination. *Nat. Immunol.* **2011**, *12*, 509−517.
(52) Coffman, R. L.; Sher, A.; Seder, R. A. Vaccine Adjuvants: Putting Innate Immunity to Work. *Immunity* **2010**, *33*, 492−503.
(53) Mbow, M. L.; Gregorio, E. de; Valiante, N. M.; Rappuoli, R. New Adjuvants for Human Vaccines. *Curr. Opin. Immunol.* **2010**, *22*, 411−416.
(54) Irvine, D. J.; Swartz, M. A.; Szeto, G. L. Engineering Synthetic Vaccines Using Cues from Natural Immunity. *Nat. Mater.* **2013**, *12*, 978−990.
(55) Moyer, T. J.; Kato, Y.; Abraham, W.; Chang, J. Y. H.; Kulp, D. W.; Watson, N.; Turner, H. L.; Menis, S.; Abbott, R. K.; Bhiman, J. N.; Melo, M. B.; Simon, H. A.; Herrera-De la Mata, S.; Liang, S.; Seumois, G.; Agarwal, Y.; Li, N.; Burton, D. R.; Ward, A. B.; Schief, W. R.; Crotty, S.; Irvine, D. J. Engineered Immunogen Binding to Alum Adjuvant Enhances Humoral Immunity. *Nat. Med.* **2020**, *26*, 430−440.
(56) Frens, G. Controlled Nucleation for the Regulation of the Particle Size in Monodisperse Gold Suspensions. *Nature, Phys. Sci.* **1973**, *241*, 20−22.
(57) Perrault, S. D.; Chan, W. C. W. Synthesis and Surface Modification of Highly Monodispersed, Spherical Gold Nanoparticles of 50−200 nm. *J. Am. Chem. Soc.* **2009**, *131*, 17042−17043.
(58) Schneider, C. A.; Rasband, W. S.; Eliceiri, K. W. NIH Image to ImageJ: 25 Years of Image Analysis. *Nat. Methods* **2012**, *9*, 671−675.

https://dx.doi.org/10.1021/acsnano.0c02240
ACS Nano XXXX, XXX, XXX−XXX